Magnetoelectric Effect in an XY-like Spin Glass System $Ni_xMn_{1-x}TiO_3$

Y. Yamaguchi,[1] T. Nakano,[2] Y. Nozue,[2] and T. Kimura[1]

[1]*Division of Materials Physics, Graduate School of Engineering Science, Osaka University, Toyonaka, Osaka 560-8531, Japan*
[2]*Department of Physics, Graduate School of Science, Osaka University, Toyonaka, Osaka 560-0043, Japan*

(Received 12 July 2011; published 30 January 2012)

Magnetoelectric (ME) properties were investigated for an XY-like spin glass (SG) system, $Ni_xMn_{1-x}TiO_3$ with an ilmenite structure. The ME effect is usually observed in systems with peculiar couplings between a crystal lattice and a magnetic order. Nonetheless, we found an antisymmetric ME effect with nonzero ME tensor elements below $T_{ME} = 8$–10 K in samples showing SG transitions. At T_{ME}, no specific heat anomaly was observed, suggesting the absence of long-range magnetic order. We discuss the origin of the ME effect in the XY-like SG system in terms of an alignment of toroidal moments.

DOI: 10.1103/PhysRevLett.108.057203 PACS numbers: 75.50.Lk, 75.10.Nr, 75.47.Lx, 75.85.+t

Interest in the study of magnetoelectric (ME) effects, magnetic control of electric polarization P or electric control of magnetization M, has been reinvigorated since the discovery of spin-driven ferroelectricity and giant ME effects in some spin-spiral magnets [1,2]. Usually, the ME effect can exist in crystals with *ordered* spin structures having peculiar magnetic symmetries. In ME materials, additional multispin variables often play an important role in their ME properties. A well-known multispin variable which couples spins with P is ''vector spin chirality,'' defined as $\boldsymbol{\kappa} = (\boldsymbol{S}_i \times \boldsymbol{S}_j)$, where $\boldsymbol{S}_i$ and $\boldsymbol{S}_j$ denote spins at the sites i and j. The most successful microscopic mechanisms for the contribution of $\boldsymbol{\kappa}$ to the spiral-spin-driven ferroelectricity are the spin-current [3] and the inverse Dzyaloshinskii-Moriya [4] mechanisms. Another known ME active multispin variable is toroidal moment $\boldsymbol{t}$, which is described as the outer product of the displacement of magnetic ions from the center position $\boldsymbol{r}_i$ and their spins $\boldsymbol{S}_i$; i.e., $\boldsymbol{t} \propto \Sigma_i \boldsymbol{r}_i \times \boldsymbol{S}_i$ [5,6]. The sign of $\boldsymbol{t}$ changes under time-reversal and space-inversion operation, and ME effects in several compounds such as $Ga_{2-x}Fe_xO_3$ have been discussed in terms of the toroidal ordering [7–9].

Theoretically, these multispin variables can be nonzero even in the absence of long-range magnetic order. An example of such a situation is the ''chiral spin liquid phase'' in some helimagnets [10,11]. Another example is the ''spin-chirality decoupling'' in spin glass (SG) systems, which was originally discussed for the scalar spin chirality in Heisenberg SG systems [12] but has also been applied to the vector spin chirality in XY-like SG systems recently [13]. Thus, it is possible that ME materials are found in magnetically disordered systems. However, most of the previous experimental studies on magnetoelectricity have been done on materials showing long-range magnetic orders. There are few reports on ME effects in magnetically disordered systems, except for the multiglass system $(Sr, Mn)TiO_3$ [14].

In this Letter, we pursue the ME coupling owing to multispin variables in magnetically disordered systems. Especially in the XY-like SG systems, noncollinear spin configurations confined within the XY plane are possible and might align the ME active multispin variables such as $\boldsymbol{\kappa}$ and $\boldsymbol{t}$. For this purpose, we choose ilmenite-type $Ni_xMn_{1-x}TiO_3$ and carry out detailed measurements of its ME properties. We found antisymmetric ME effects in samples showing XY-like SG character and discuss the origin of the ME effect in terms of an alignment of toroidal moments.

$Ni_xMn_{1-x}TiO_3$ with an ilmenite structure crystallizes in the centrosymmetric space group $R\bar{3}$ in which a (Ni,Mn) plane and a Ti plane are alternately stacked along the hexagonal c axis. Randomly distributed magnetic Ni^{2+} and Mn^{2+} ions in each (Ni,Mn) plane form a honeycomb lattice. Figure 1(a) shows the magnetic phase diagram determined by previous M and neutron diffraction measurements [15,16]. An end compound, $MnTiO_3$ [17], exhibits an antiferromagnetic (AFM) order with the easy axis along the c axis below $T_N \approx 64$ K. In each Mn plane, the coupling between nearest-neighboring Mn moments is AFM. The AFM structure is illustrated in Fig. 1(b) and termed ''AFM1.'' The other end compound, $NiTiO_3$ [17], shows another AFM order (AFM3) below $T_N \approx 23$ K. In the AFM3 phase, Ni moments are ferromagnetically coupled within each Ni plane but antiferromagnetically between adjacent Ni planes [Fig. 1(d)]. The Ni moments in the AFM3 phase lie in the plane, unlike the AFM1 phase in $MnTiO_3$. Thus, for mixed $Ni_xMn_{1-x}TiO_3$, AFM Mn-Mn and ferromagnetic Ni-Ni bonds are randomly distributed in the (Mn,Ni) honeycomb lattice, which causes competing magnetic interactions and a resultant SG state at around $x = 0.40$–0.48. In addition, the competition of spin anisotropy yields the effective easy plane anisotropy, and then the SG state becomes an XY-type one [18].

Single crystals of $Ni_xMn_{1-x}TiO_3$ $(0.38 \leq x \leq 0.44)$ were prepared by the floating zone method, as reported previously [19]. For measurements of electric polarization P and relative dielectric constant ε, the crystals were cut into a thin plate shape (approximately 40 $mm^2 \times 0.1$ mm)

 © 2012 American Physical Society

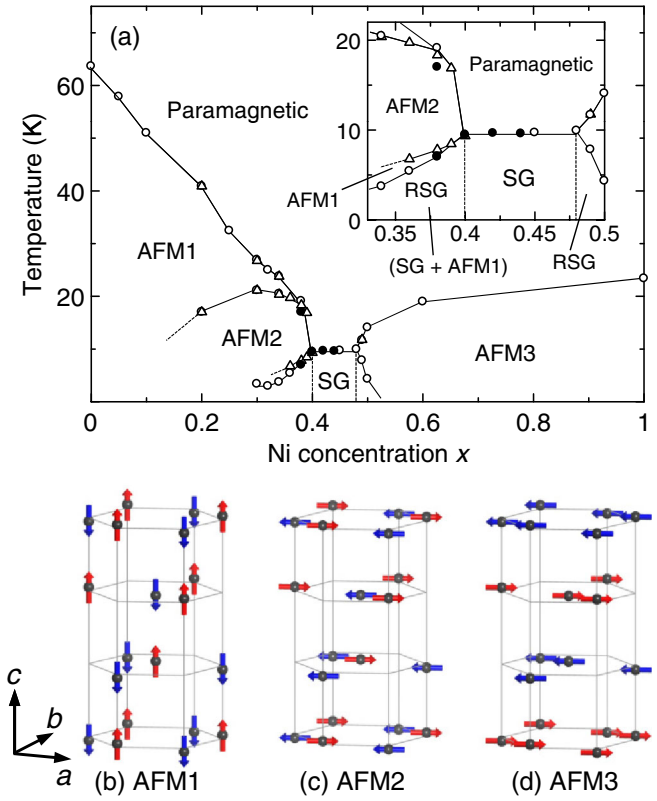

FIG. 1 (color online). (a) Magnetic phase diagram of $Ni_xMn_{1-x}TiO_3$ reproduced from Refs. [15,16]. Open circles and open triangles represent transition temperatures determined from previous M and neutron diffraction measurements, respectively. Closed circles represent results of our M measurements. Inset of (a): an expanded view. (b)–(d) Magnetic structures of the AFM1, AFM2, and AFM3 phases, respectively. Thick arrows denote (Ni,Mn) spins and are color-coded according to their relative directions.

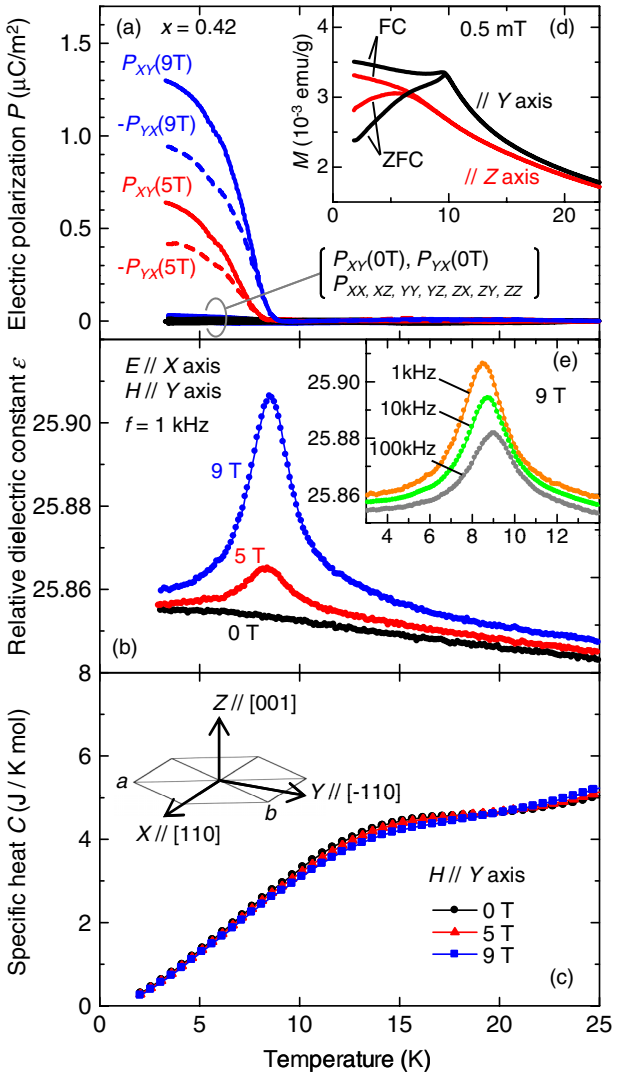

FIG. 2 (color online). T profiles of (a) P along the X, Y, and Z axes at H along X, Y, and Z; (b) ε along X at H along Y; and (c) C at H along Y for the $x = 0.42$ sample. Inset of (c): the definitions of the X, Y, and Z axes. (d) T dependence of zero-field-cooled (ZFC) and field-cooled (FC) M along the Y and Z axes at 0.5 mT. (e) ε at several frequencies and $\mu_0 H = 9$ T.

with the widest faces parallel to the (001), (110), or (− 110) plane. Silver electrodes were vacuum deposited onto these faces. We measured ε using an LCR meter with a frequency (f) range from 1 to 100 kHz. The temperature (T) and magnetic field (H) profiles of P were obtained by time integration of pyroelectric and ME currents measured with an electrometer upon T sweeping and H sweeping, respectively. Measurements of magnetization M were carried out with a commercial magnetometer. Specific heat C was measured by the relaxation method.

First, we focus on the results of an $x = 0.42$ sample showing the XY-like SG behavior [20]. As seen in Fig. 2(d), two successive SG transitions at $T_{SG1} \approx 9.6$ K for M along the Y axis and $T_{SG2} \approx 6.0$ K for M along the Z axis are evident, which is consistent with a previous result [18] and characteristic of SG systems with an easy plane anisotropy [21]. Here, the definitions of the X, Y, and Z axes are illustrated in the inset of Fig. 2(c). Figures 2(a)–2(c) show the T profiles of P, ε, and C in selected magnetic fields, respectively. Subscripts of P denote measurement settings; for example, P_{XY} is P along the X axis in H along the Y axis. We measured P upon a warming process without an electric field E after cooling the sample at $\mu_0 H = 9$ T and $E = 0.5$ MV/m from 30 to 3 K (ME cooling). As seen in Fig. 2(a), no finite P was observed in the absence of H. However, P is induced by applying H below $T_{ME} \approx 8$ K for 5 T and ≈ 8.5 K for 9 T only at off-diagonal components P_{XY} and P_{YX}. This means that the ME effect is observed in the sample showing SG transitions. The opposite sign and almost the same magnitude between P_{XY} and P_{YX} indicate the antisymmetric relation, $P_{XY} = -P_{YX}$. By using the ME tensor elements, the ME effect is expressed as

$$\begin{pmatrix} 0 & \alpha_{XY} & 0 \\ -\alpha_{XY} & 0 & 0 \\ 0 & 0 & 0 \end{pmatrix}.$$

The off-diagonal and antisymmetric ME effect seems to reflect the symmetry of the XY SG system. (More precisely, the magnitudes of P_{XY} and P_{YX} are slightly different. One of the reasons for the difference may be due to measurement errors for the electrode area. Another more significant reason is the presence of the remarkable ME-cooling-condition dependence of P in the XY-like SG system [20].)

Note that the magnetic point group of the AFM1 phase observed in the Mn-rich region is $\bar{3}'$, which allows the linear ME effect with the ME tensor elements $\alpha_{XX} = \alpha_{YY}$, $\alpha_{XY} = -\alpha_{YX}$, and α_{ZZ} [22]. In fact, finite α_{ZZ} has been experimentally confirmed in an $x = 0$ sample [23]. It is important to clarify the differences between the ME effects of the AFM1 samples and the $x = 0.42$ SG samples. The ME tensor components of the $x = 0.42$ sample did not contain any diagonal components (α_{XX}, α_{YY}, or α_{ZZ}), suggesting that the ME effect observed in the $x = 0.42$ SG sample is ascribed to a different origin from that in the AFM1 samples.

Figure 2(b) shows the T profiles of ε along the X axis. At 0 T, no anomaly was observed at any of the measured frequencies. By contrast, at 5 and 9 T, a sharp peak anomaly appears in the $\varepsilon - T$ curves. As seen in Fig. 2(e), the peak position is at around T_{ME} and monotonically shifts toward higher temperatures with increasing f. Furthermore, the peak height decreases as f increases. These features resemble those of the ac magnetic susceptibility in spin glasses or the ac dielectric constant in relaxor ferroelectrics [20], suggesting that a magnetoelectrically glassy state contributes to the observed ME effect.

The above results show that the ME effect is observed in the samples showing the SG transition, which indicates that some order parameter develops in the SG system. One of the possible origins of the ME effect is the formation of a long-range magnetic order induced by applied H. To examine whether there is the H-induced long-range magnetic order, we measured the specific heat C. Figure 2(c) displays the T dependence of C at several magnetic fields applied along the Y axis. At 0 T, C shows no anomaly at $T_{\mathrm{SG1}} \approx 9.6$ K or $T_{\mathrm{SG2}} \approx 6.0$ K but exhibits a broad peak at around 15 K ($> T_{\mathrm{SG}}$). The broad peak is slightly suppressed by applying H. Similar features are often observed in SG systems such as canonical SG CuMn [24] and insulating SG (Eu,Sr)S [25]. We emphasize that C in the $x = 0.42$ sample did not show any anomaly at T_{ME}, indicating that there is no H-induced long-range magnetic order in the $x = 0.42$ sample.

Here, we discuss the origin of the ME effect in the XY-like SG system in terms of toroidal moment $\boldsymbol{t}$ [5]. When $\boldsymbol{t}$ is finite, antisymmetric ME effects can be allowed, i.e., $\boldsymbol{P} \propto -\boldsymbol{t} \times \boldsymbol{H}$ and $\boldsymbol{M} \propto \boldsymbol{t} \times \boldsymbol{E}$, which are obtained from the free energy expansion analysis [6]. Figure 3(a) illustrates a (Ni,Mn) honeycomb lattice of (Ni, Mn)TiO_3. If spins whose directions are confined within the XY plane freeze in a completely random manner, $\boldsymbol{t}$ ($\propto \Sigma_i \boldsymbol{r}_i \times \boldsymbol{S}_i$) all over the lattice becomes zero statistically. However, if both E along the X axis (E_X) and H along the Y axis (H_Y) are present during the spin-freezing process (i.e., ME cooling), it is expected that $\boldsymbol{t}$ is polarized along the Z axis (t_Z) through the coupling of $\boldsymbol{t} \cdot (\boldsymbol{E} \times \boldsymbol{H})$. This means that vortexlike arrays of spins, as illustrated in Figs. 3(b) and 3(c), are induced by the ME cooling and frozen below T_{SG}. Note that, to yield finite t_Z, it is not necessary for spins to be perfectly arranged in a vortex manner. It is sufficient for them to have a finite vortexlike component. This scenario reasonably explains the antisymmetric ME effect observed in the $x = 0.42$ sample.

To further test the validity of the toroidal scenario, we measured the H dependence of P_{XY} after two different ME cooling procedures. Figure 3(d) shows the data measured at 2 K after cooling at $+E_X$ and $+H_Y$ (black line), and cooling at $-E_X$ and $+H_Y$ (gray line). The $P - H$ curves

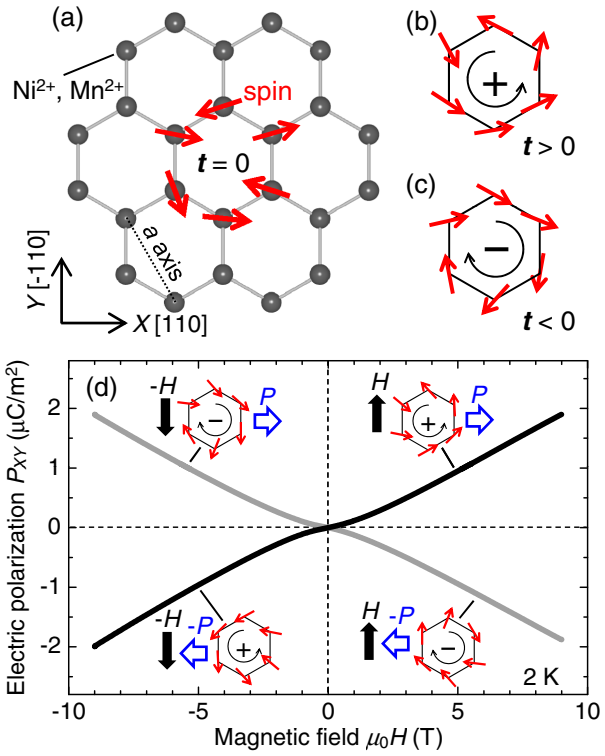

FIG. 3 (color online). (a) A (Mn,Ni) honeycomb lattice with randomly frozen spins. (b),(c) Schematic diagrams of spin configurations with finite + and − toroidal moments on the honeycomb lattice, respectively. (d) H dependence of P_{XY} at 2 K. Black and gray lines represent the data measured after the ME cooling at $E_X = +0.5$ MV/m and $\mu_0 H_Y = 9$ T, and at $E_X = -0.5$ MV/m and $\mu_0 H_Y = 9$ T, respectively. Illustrations in (d) represent possible relationships among the toroidal moment, applied H, and induced P at the respective situations.

are odd functions to H and monotonically increase (or decrease) with increasing H. Furthermore, by changing the sign of the poling E_X, that of P_{XY} is also reversed. In the toroidal scenario, the reversal of P is equivalent to the reversal of $\boldsymbol{t}$. Considering the spin and toroidal configurations in the (Ni,Mn) honeycomb lattice illustrated in the insets of Fig. 3(d), the observed features can be explained by the toroidal scenario. This interpretation is also consistent with the presence of the ME effect in the magnetically disordered XY SG system.

Although the toroidal scenario successfully explains the ME effect of the $x = 0.42$ SG sample, we further investigated the ME properties of samples with other compositions ($0.38 \leq x \leq 0.44$). As seen in the inset of Fig. 1(a), the phase diagram of the Mn-rich side ($x < 0.4$) is complicated. For example, the $x = 0.38$ sample shows three successive magnetic transitions. The first transition is an AFM transition into a phase in which spins are ordered in the same manner as AFM1, but their direction is within the XY plane ["AFM2," shown in Fig. 1(c)] [15,16]. As T decreases, the spin direction varies and a magnetic transition into the AFM1 phase occurs at ~8 K. Moreover, the $x = 0.38$ sample undergoes a reentrant spin glass (RSG) transition at ~7 K. According to a former study [16], the SG and AFM1 phases coexist in the RSG phase.

Figure 4(a) displays the T profiles of P_{XY} for samples with $x = 0.38$–0.44 at 9 T. The RSG sample with $x = 0.38$ also exhibits finite P_{XY}, accompanied by the AFM ordering below $T_N \approx 17$ K. As T decreases, P_{XY} shows a dip at ~9 K and increases again below ~9 K. The observed ME tensor at $T = 9$–17 K is nonzero not only in the off-diagonal P_{XY} (and P_{YX}) but also in the diagonal P_{XX} [Fig. 4(b)], which is consistent with the magnetic point group $\bar{1}'$ of the AFM2 structure [22]. As seen in Fig. 4(b), however, the diagonal P_{XX} due to the AFM2 order disappears at the RSG phase ($T < \sim 9$ K), which is the same as the ME effect observed in SG samples. These results indicate that the ME effect of SG samples is differentiated from that due to the AFM2 ordering. Furthermore, the magnitude of P_{XY} in the SG samples shows the maximum at $x = 0.40$ and decreases at $x > 0.40$ with increasing x. Then, at $x = 0.44$, P_{XY} almost disappears [but is still finite (≈ 0.05–0.15 μC/m^2 depending on the ME cooling condition) below 7 K], although the sample also shows the SG transition. Presently, we do not have a clear explanation for the suppression of the ME effect with increasing x in the SG phase. However, the suppression of P_{XY} (and/or the increase of the stiffness to align toroidal moment $\boldsymbol{t}$) with increasing x can be partly explained in terms of the suppression of $\boldsymbol{t}$ ($\propto \Sigma_i \boldsymbol{r}_i \times \boldsymbol{S}_i$) by replacing Mn^{2+} ions ($S = 5/2$) with Ni^{2+} ions ($S = 1$).

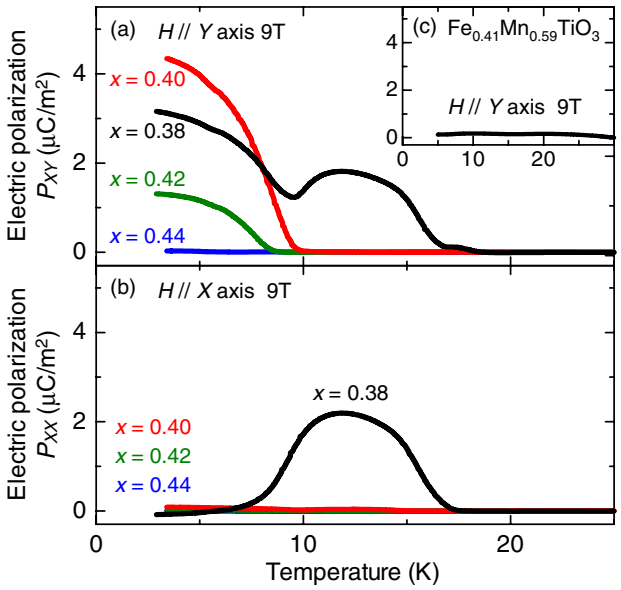

FIG. 4 (color online). T dependence of (a) P_{XY} and (b) P_{XX} at 9 T for $Ni_xMn_{1-x}TiO_3$ ($0.38 \leq x \leq 0.44$). The data shown in (a),(b) correspond to the ME tensor elements α_{XY} and α_{XX}, respectively. (c) T dependence of P_{XY} at 9 T for $Fe_{0.41}Mn_{0.59}TiO_3$.

Finally, we compare the ME effect of $Ni_xMn_{1-x}TiO_3$ and that of $Fe_xMn_{1-x}TiO_3$ known as an Ising SG [26,27]. Because of the Ising nature, which is ascribed to a strong single-ion anisotropy of Fe^{2+}, noncollinear spin configurations and vortexlike arrays, as shown in Fig. 3(b), cannot be expected in SG $Fe_xMn_{1-x}TiO_3$. Thus, we will not observe an ME effect in $Fe_xMn_{1-x}TiO_3$. To confirm this expectation, we measured P_{XY} for a single crystal of $Fe_{0.41}Mn_{0.59}TiO_3$, which shows a typical Ising SG behavior below $T_{SG} \approx 23$ K [27] and has the same x level as the ME $Ni_xMn_{1-x}TiO_3$ studied here. As displayed in Fig. 4(c), no ME effect was observed. This result suggests that the ME effect in $Ni_xMn_{1-x}TiO_3$ is ascribed to the XY-like SG character and further supports the toroidal scenario.

In summary, we investigated magnetoelectric properties of $Ni_xMn_{1-x}TiO_3$. We found off-diagonal and antisymmetric ME effects in samples showing XY-like spin glass character. The magnetoelectric effects were reasonably explained by considering that the spin-freezing process under both electric and magnetic fields makes toroidal moments polarized. To further verify the polarization of toroidal moments, it is desirable to apply some optical techniques (e.g., magnetochiral dichroism and nonreciprocal x-ray gyrotropy) which allow the observation of simultaneous breaking of space-inversion and time-reversal symmetries [6]. Furthermore, similar magnetoelectric properties could be expected in other XY-like spin glasses such as $Rb_2(Mn, Cr)Cl_4$ [28] if the necessary conditions in terms of symmetry are fulfilled. Our results suggest that studies of magnetoelectric properties in a magnetically disordered system provide an opportunity to study multi-spin variables by their separation from the ordering of spins.

We thank T. Taniguchi, H. Kawamura, G. L. J. A. Rikken, and A. Ito for their enlightening discussions.

This work was supported by KAKENHI (20674005, 20001004, and 19052001) and the Global COE Program (G10).

[1] S.-W. Cheong and M. V. Mostovoy, Nature Mater. **6**, 13 (2007).
[2] T. Kimura, Annu. Rev. Mater. Res. **37**, 387 (2007).
[3] H. Katsura, N. Nagaosa, and A. V. Balatsky, Phys. Rev. Lett. **95**, 057205 (2005).
[4] I. A. Sergienko and E. Dagotto, Phys. Rev. B **73**, 094434 (2006).
[5] H. Schmid, Ferroelectrics **252**, 41 (2001).
[6] N. A. Spaldin, M. Fiebig, and M. Mostovoy, J. Phys. Condens. Matter **20**, 434203 (2008).
[7] Yu. F. Popov, A. M. Kadomtseva, G. P. Vorob'ev, V. A. Timofeeva, D. M. Ustinin, A. K. Zvezdin, and M. M. Tegeranchi, Zh. Eksp. Teor. Fiz. **114**, 263 (1998) [J. Exp. Theor. Phys. **87**, 146 (1998)].
[8] Yu. F. Popov, A. M. Kadomtseva, D. V. Belov, G. P. Vorob'ev, and A. K. Zvezdin, Pis'ma Zh. Eksp. Teor. Fiz. **69**, 302 (1999) [JETP Lett. **69**, 330 (1999)].
[9] I. Kornev, M. Bichurin, J.-P. Rivera, S. Gentil, H. Schmid, A. G. M. Jansen, and P. Wyder, Phys. Rev. B **62**, 12 247 (2000).
[10] S. Onoda and N. Nagaosa, Phys. Rev. Lett. **99**, 027206 (2007).
[11] F. Cinti, A. Cuccoli, and A. Rettori, Phys. Rev. B **83**, 174415 (2011).
[12] H. Kawamura, Phys. Rev. Lett. **68**, 3785 (1992).
[13] H. Kawamura, J. Phys. Condens. Matter **23**, 164210 (2011).
[14] V. V. Shvartsman, S. Bedanta, P. Borisov, W. Kleemann, A. Tkach, and P. M. Vilarinho, Phys. Rev. Lett. **101**, 165704 (2008).
[15] A. Ito, H. Kawano, H. Yoshizawa, and K. Motoya, J. Magn. Magn. Mater. **104–107**, 1637 (1992).
[16] H. Yoshizawa, H. Kawano, H. Mori, S. Mitsuda, and A. Ito, Physica (Amsterdam) **180–181B**, 94 (1992).
[17] G. Shirane, S. J. Pickart, and Y. Ishikawa, J. Phys. Soc. Jpn. **14**, 1352 (1959).
[18] H. Kawano, H. Yoshizawa, A. Ito, and K. Motoya, J. Phys. Soc. Jpn. **62**, 2575 (1993).
[19] H. Takei, J. Mater. Sci. **16**, 1310 (1981).
[20] See Supplemental Material at http://link.aps.org/supplemental/10.1103/PhysRevLett.108.057203 for more details.
[21] D. M. Cragg and D. Sherrington, Phys. Rev. Lett. **49**, 1190 (1982).
[22] R. R. Birss, *Symmetry and Magnetism* (North-Holland, Amsterdam, 1966).
[23] N. Mufti, G. R. Blake, M. Mostovoy, S. Riyadi, A. A. Nugroho, and T. T. M. Palstra, Phys. Rev. B **83**, 104416 (2011).
[24] G. E. Brodale, R. A. Fisher, W. E. Fogle, N. E. Phillips, and J. Van Curen, J. Magn. Magn. Mater. **31–34**, 1331 (1983).
[25] D. Meschede, F. Steglich, W. Felsch, H. Maletta, and W. Zinn, Phys. Rev. Lett. **44**, 102 (1980).
[26] A. Ito, H. Aruga, E. Torikai, M. Kikuchi, Y. Syono, and H. Takei, Phys. Rev. Lett. **57**, 483 (1986).
[27] H. A. Katori and A. Ito, J. Phys. Soc. Jpn. **62**, 4488 (1993).
[28] K. Katsumata, J. Tuchendler, Y. J. Uemura, and H. Yoshizawa, Phys. Rev. B **37**, 356 (1988).